A regularised continuum damage model based on the mesoscopic scale for soft tissue

Sergio Blanco , César Andrés Polindara, Jose María Goicolea

A B S T R A C T

Material properties of soft fibrous tissues are highly conditioned by the hierarchical structure of this kind of composites. Collagen based tissues present, at decreasing length scales, a complex framework of fibres, fibrils, tropocollagen molecules and amino-acids. Understanding the mechanical behaviour at nano-scale level is critical to accurately incorporate this structural information in phenomenological damage models. In this work we derive a relationship between the mechanical and geometrical properties of the fibril constituents and the soft tissue material parameters at macroscopic scale. A Hodge–Petruska two-dimensional model has been used to describe the fibrils as staggered arrays of tropocollagen molecules. After a mechanical characterisation of each of the fibril components, two fibril failures modes have been defined related with two planes of weakness. A phenomenological continuous damage model with regularised softening was presented along with meso-structurally based definitions for its material parameters. Finally, numerical analysis at fibril, fibre and tissue levels are presented to show the capabilities of the model.

1. Introduction

Soft tissues have a hierarchical structure with several scales, from the amino-acids forming the proteins in the atomistic scale to the arterial walls in the continuum scale. The elementary building block of the fibrous reinforcement in soft tissues is collagen. This structural protein consists of tropocollagen (TC) molecules with an aspect ratio close to 200. TC molecules are disposed in staggered arrays forming fibrils which are organised in families of fibres surrounded by an almost incompressible ground matrix (see Baer et al., 1991; Sasaki and Odajima, 1996; Buehler, 2008; Gautieri et al., 2011 among others).

Degradation phenomena in soft tissues have been successfully reproduced through phenomenological damage models (see Balzani et al., 2006; Calvo et al., 2007; Ehret and Itskov, 2009; Peña et al., 2010 among others) although some plasticity-based models have also been presented (see Tanaka and Yamada, 1990; Gasser and Holzapfel, 2002; Itskov and Aksel, 2004). The capabilities and accuracy of these phenomenological models for soft tissues have been improving in the past years. However, less effort has been paid to develop continuum models based on the underlying fracture mechanisms at molecular scale.

The structural mechanisms that control the degradation of soft tissues are related with the behaviour of their fundamental constituents. The study of the relationship between the molecular and intermolecular properties and the tissue behaviour is been actively addressed at present (Buehler, 2006b, 2008; Shoulders and Raines, 2009; Gautieri et al., 2011; Shen et al., 2011 among others). As a consequence, several damage models for soft tissues have been presented derived from the molecular features associated with the tropocollagen molecules. A stochastic, structurally based damage model that considers statistical aspects related to the length distribution of the reinforcing fibres was presented in Rodríguez et al. (2006). A reactive mesoscopic model was presented in Buehler (2008), where tropocollagen molecules are described as a collection of particles interacting according to multibody potentials (see also Buehler, 2006a). Based on these molecular simulations, a multiscale, plasticity based, constitutive model was presented in Tang et al. (2010). Another plasticity based model has been presented in Gasser (2011), where viscoplastic sliding of collagen fibrils is associated with the irreversible degradation of the proteoglycan bridges between them. This model has been applied to the study of the properties of the infrarenal aorta in Martufi and Gasser (2011) and has been enriched with a collagen turnover model in Martufi and Gasser (2012).

In this work we consider the soft tissue as a fibre reinforced composite and the fibre as a fibril reinforced composite. We want

to physically motivate the irreversible deformation of soft tissues beyond the physiological range of loading. The goal is to explain the damage mechanisms in the fibres using the evolution of their inner structure. In order to do so we assume, as a hypothesis, that inelastic phenomena in the fibre are caused only by degradation processes in the fibrils (Tang et al., 2010). Firstly, we characterise the geometrical and mechanical properties of the fibre components at molecular scale, *i.e.* the tropocollagen molecules in the fibril and the cohesive forces between them. Afterwards, we identify the onset of damage with the development of planes of weakness along the unions between TC molecules. We obtain the macroscale parameters of the fibre from the mesoscale level by numerical homogenisation. In order to pass hierarchically the parameters we have to estimate volume fractions of the fibril within the fibre and of the fibre within the tissue. We have characterised the following macroscopic material parameters of the fibre: the yield strength, the total dissipation energy and the initial size of the elastic domain (that depends on the stored elastic energy density at the onset of damage). Finally we use these structure-derived material parameters to fully characterise a continuum damage model for the fibres. The parameters of this continuum damage model are thus based on the mesoscopic mechanisms within the fibre when irreversible processes take place.

The paper is organised as follows. In Section 2 the methods used in this work are presented: a local damage model for fibrous materials with regularised softening and a mesoscopic-based structural characterisation of the inelastic behaviour of the fibres. Several numerical simulations are included in Section 3, where we perform mechanical analysis at fibril, fibre and tissue levels (all the hierarchical scales we have considered). Finally Section 4 includes the main conclusions of the work.

2. Methods

2.1. A local damage model with regularised softening

We present a material damage model suited for fibrous materials. As stated in Peña et al. (2009), this kind of continuous damage models can reproduce the Mullins' effect only after damage initiation. Two main hypothesis have been considered: the damage processes depend only on the isochoric deformation and each material phase, ground matrix and fibres, damages independently. The model presented here needs only three parameters to characterise the material softening in each phase of the composite: a threshold value that defines the initial size of the elastic domain (usually a limit value of the Cauchy stress or the stretch in the uniaxial homogeneous tension test), a parameter that defines the total amount of internal dissipated energy and a coefficient that affects the rate of softening.

2.1.1. Kinematics

Let $\mathcal{B}_0$ be the reference configuration of the body of interest and $\mathcal{B}_t$ its current configuration. The mapping $\varphi(\boldsymbol{X},t):\mathcal{B}_0\times\mathbb{R}^+\to\mathcal{B}_t$ defines the motion that transforms, at time t, position vectors of the material points $\boldsymbol{X}\in\mathcal{B}_0$ into spatial position vectors $\boldsymbol{x}=\varphi(\boldsymbol{X},t)\in\mathcal{B}_t$. The deformation gradient is defined as $\boldsymbol{F}(\boldsymbol{X},t)=\partial\varphi(\boldsymbol{X},t)/\partial\boldsymbol{X}$, which is multiplicatively decomposed into dilatational and distortional (isochoric) parts (Flory, 1961):

$$\boldsymbol{F}=J^{1/3}\overline{\boldsymbol{F}};\quad \overline{\boldsymbol{F}}=J^{-1/3}\boldsymbol{F}. \tag{1}$$

Eq. (1) allows to obtain the right and left Cauchy–Green deformation tensors, $\boldsymbol{C}$ and $\boldsymbol{b}$, and their corresponding isochoric counterparts:

$$\boldsymbol{C}=\boldsymbol{F}^{\mathrm{T}}\boldsymbol{F}=J^{-2/3}\overline{\boldsymbol{F}}^{\mathrm{T}}\overline{\boldsymbol{F}}=J^{-2/3}\overline{\boldsymbol{C}}, \tag{2}$$

$$\boldsymbol{b}=\boldsymbol{F}\boldsymbol{F}^{\mathrm{T}}=J^{-2/3}\overline{\boldsymbol{F}}\overline{\boldsymbol{F}}^{\mathrm{T}}=J^{-2/3}\overline{\boldsymbol{b}}. \tag{3}$$

If we consider n_f families of fibres, the direction of each family at point $\boldsymbol{X}\in\mathcal{B}_0$ is defined by the unit vector $\boldsymbol{a}_{0i}$, with $i=\{1,n_{\mathrm{f}}\}$. The description of these vectors in the current configuration is:

$$\boldsymbol{a}_i=\boldsymbol{F}\,\boldsymbol{a}_{0i};\quad \bar{\boldsymbol{a}}_i=\overline{\boldsymbol{F}}\,\boldsymbol{a}_{0i};\quad \|\boldsymbol{a}_{0i}\|=1, \tag{4}$$

where the macroscopic stretches in the direction of the family of fibres i are defined by $\lambda_i=\|\boldsymbol{a}_i\|>0$ and $\bar{\lambda}_i=\|\bar{\boldsymbol{a}}_i\|>0$. This structure is characterised by a set of generalised structure symmetric tensors (Holzapfel et al., 2000) expressed as:

$$\boldsymbol{H}_i=\boldsymbol{a}_{0i}\otimes\boldsymbol{a}_{0i},\quad i=\{1,n_{\mathrm{fibres}}\}. \tag{5}$$

We assume henceforth our domain of interest has a quasi-incompressible constitutive behaviour and that there are only two families of fibres. The definition of the standard invariants (Spencer, 1971) associated with the distortional deformation

$$\bar{I}_1=\mathrm{tr}\left(\overline{\boldsymbol{C}}\right)=\mathrm{tr}\left(\overline{\boldsymbol{b}}\right)=J^{-2/3}I_1, \tag{6}$$

$$\bar{I}_2=\frac{1}{2}\left[\mathrm{tr}\left(\overline{\boldsymbol{C}}\right)^2-\mathrm{tr}\left(\overline{\boldsymbol{C}}^2\right)\right]=\frac{1}{2}\left[\mathrm{tr}\left(\overline{\boldsymbol{b}}\right)^2-\mathrm{tr}\left(\overline{\boldsymbol{b}}^2\right)\right]=J^{-4/3}I_2, \tag{7}$$

$$\bar{I}_3=\det\overline{\boldsymbol{C}}=\det\overline{\boldsymbol{b}}=1, \tag{8}$$

$$J=(\det\overline{\boldsymbol{C}})^{1/2}=(\det\overline{\boldsymbol{b}})^{1/2}, \tag{9}$$

$$\bar{I}_4=\overline{\boldsymbol{C}}:\boldsymbol{H}_1=\overline{\boldsymbol{C}}:(\boldsymbol{a}_{01}\otimes\boldsymbol{a}_{01}), \tag{10}$$

$$\bar{I}_6=\overline{\boldsymbol{C}}:\boldsymbol{H}_2=\overline{\boldsymbol{C}}:(\boldsymbol{a}_{02}\otimes\boldsymbol{a}_{02}) \tag{11}$$

allows us to define the following Green–Lagrange strain-like quantities:

$$\overline{E}_1=\overline{\boldsymbol{C}}:\boldsymbol{H}_1-1=\bar{I}_4-1, \tag{12}$$

$$\overline{E}_2=\overline{\boldsymbol{C}}:\boldsymbol{H}_2-1=\bar{I}_6-1, \tag{13}$$

which characterise the strain in the direction of the mean orientations $\boldsymbol{a}_{01}$ and $\boldsymbol{a}_{02}$ (Gasser et al., 2006).

2.1.2. Strain energy function and stress response

Based on the kinematic description of Eq. (1), the strain energy density function can be defined in a decoupled form with a dilatational and an isochoric part. The isochoric contribution can also be decomposed into a part associated with the isotropic behaviour of the ground matrix and a part associated with the anisotropic behaviour of the fibres as:

$$W=U(J)+(1-d_g)\overline{W}_g(\overline{\boldsymbol{C}})+(1-d_{f1})\overline{W}_{f1}(\overline{\boldsymbol{C}},\boldsymbol{H}_1)+(1-d_{f2})\overline{W}_{f2}(\overline{\boldsymbol{C}},\boldsymbol{H}_2), \tag{14}$$

where $\overline{W}_g$, $\overline{W}_{f1}$ and $\overline{W}_{f2}$ represent, respectively, the effective strain energy functions of the hypothetical undamaged materials matrix and fibres. These functions must obey the principle of objectivity and material frame indifference (Holzapfel and Ogden, 2010). Reduction factors $(1-d_g)$, $(1-d_{f1})$ and $(1-d_{f2})$, initially proposed in Kachanov (1958), incorporate the inelastic degradation phenomena taking place separately in the matrix and in each family of fibres, satisfying $0\leqslant d_\alpha\leqslant 1$ for $\alpha=\{g,f1,f2\}$.

Eq. (14) can be expressed in terms of the strain invariants defined in Eqs. (6)–(11) as:

$$W=U(J)+(1-d_g)\overline{W}_g(\bar{I}_1,\bar{I}_2)+(1-d_{f1})\overline{W}_{f1}(\bar{I}_1,\bar{I}_4)+(1-d_{f2})\overline{W}_{f2}(\bar{I}_1,\bar{I}_6). \tag{15}$$

We use the neo-Hookean strain energy function to reproduce the behaviour of the ground matrix and the function proposed in the Holzapfel–Gasser–Ogden model (Holzapfel et al., 2000) to reproduce the behaviour of each family of fibres. Eq. (15) is thus particularised as:

$$W = \underbrace{\frac{1}{2}K(J-1)^2}_{U(J)} + (1-d_g)\underbrace{\frac{1}{2}c(\bar{I}_1-3)}_{\overline{W}_g} + (1-d_{f1})\underbrace{\frac{k_{11}}{2k_{21}}\left(e^{k_{21}\overline{E}_1^2}-1\right)}_{\overline{W}_{f1}} + (1-d_{f2})\underbrace{\frac{k_{12}}{2k_{22}}\left(e^{k_{22}\overline{E}_2^2}-1\right)}_{\overline{W}_{f2}}, \quad (16)$$

where K can be interpreted as a penalty parameter that enforces incompressibility, $\{c, k_{11}, k_{21}, k_{12}, k_{22}\}$ are material parameters and $\{\overline{E}_1, \overline{E}_2\}$, previously defined in (12) and (13), represent the deformation along the mean fibre orientations $\boldsymbol{a}_{01}$ and $\boldsymbol{a}_{02}$.

We apply the standard Coleman–Noll procedure (Coleman and Noll, 1963; Coleman and Gurtin, 1967) to obtain the stress response and the model internal dissipation. We particularise the second law of thermodynamics through the Clausius–Plank inequality for isothermal processes

$$\mathcal{D}_{\text{INT}} = \boldsymbol{S} : \frac{1}{2}\dot{\boldsymbol{C}} - \dot{W}, \quad (17)$$

where the rate of change of W is derived using the chain rule as:

$$\dot{W} = \left(\frac{\partial U}{\partial \boldsymbol{C}} + (1-d_g)\frac{\partial \overline{W}_g}{\partial \boldsymbol{C}} + (1-d_{f1})\frac{\partial \overline{W}_{f1}}{\partial \boldsymbol{C}} + (1-d_{f2})\frac{\partial \overline{W}_{f2}}{\partial \boldsymbol{C}}\right) : \dot{\boldsymbol{C}} - \dot{d}_g\overline{W}_g - \dot{d}_{f1}\overline{W}_{f1} - \dot{d}_{f2}\overline{W}_{f2}. \quad (18)$$

We deduce from Eqs. (17) and (18) the constitutive equation and the expression of the non-negative internal dissipation as:

$$\boldsymbol{S} = 2\left(\frac{\partial U}{\partial \boldsymbol{C}} + (1-d_g)\frac{\partial \overline{W}_g}{\partial \boldsymbol{C}} + (1-d_{f1})\frac{\partial \overline{W}_{f1}}{\partial \boldsymbol{C}} + (1-d_{f2})\frac{\partial \overline{W}_{f2}}{\partial \boldsymbol{C}}\right), \quad (19)$$

$$\mathcal{D}_{\text{INT}} = \dot{d}_g\overline{W}_g + \dot{d}_{f1}\overline{W}_{f1} + \dot{d}_{f2}\overline{W}_{f2} \geqslant 0. \quad (20)$$

If we use Eq. (16) to particularise Eq. (19) we obtain the second Piola–Kirchhoff stress tensor:

$$\boldsymbol{S} = \boldsymbol{S}_{\text{VOL}} + (1-d_g)\overline{\boldsymbol{S}}_g + (1-d_{f1})\overline{\boldsymbol{S}}_{f1} + (1-d_{f2})\overline{\boldsymbol{S}}_{f2}, \quad (21)$$

$$= \boldsymbol{S}_{\text{VOL}} + (1-d_g)J^{-2/3}\mathbb{P} : \widetilde{\boldsymbol{S}}_g + (1-d_{f1})J^{-2/3}\mathbb{P} : \widetilde{\boldsymbol{S}}_{f1} + (1-d_{f2})J^{-2/3}\mathbb{P} : \widetilde{\boldsymbol{S}}_{f2} \quad (22)$$

with

$$\mathbb{P}^{\mathsf{T}} = \left(\mathbb{I} - \frac{1}{3}\boldsymbol{C}^{-1}\otimes\boldsymbol{C}\right), \quad (23)$$

$$\boldsymbol{S}_{\text{VOL}} = Jp\boldsymbol{C}^{-1};\ \widetilde{\boldsymbol{S}}_g = c\boldsymbol{1}, \quad (24)$$

$$\widetilde{\boldsymbol{S}}_{f1} = 2k_{11}\overline{E}_1 e^{k_{21}\overline{E}_1^2}\boldsymbol{H}_1; \quad (25)$$

$$\widetilde{\boldsymbol{S}}_{f2} = 2k_{12}\overline{E}_2 e^{k_{22}\overline{E}_2^2}\boldsymbol{H}_2, \quad (26)$$

where $\mathbb{P}$ is the Lagrangian description of the deviatoric operator.

Applying the inverse Piola transformation (Holzapfel, 2000) in Eq. (22) enables us to obtain the Cauchy stress tensor as:

$$\boldsymbol{\sigma} = J^{-1}\boldsymbol{F}\boldsymbol{S}\boldsymbol{F}^{T}. \quad (27)$$

Eqs. (27) and (22) finally give us the following expression:

$$\boldsymbol{\sigma} = J^{-1}\boldsymbol{\tau}_{\text{VOL}} + J^{-1}(1-d_g)\mathbb{P} : \widetilde{\boldsymbol{\tau}}_g + J^{-1}(1-d_{f1})\mathbb{P} : \widetilde{\boldsymbol{\tau}}_{f1} + J^{-1}(1-d_{f2})\mathbb{P} : \widetilde{\boldsymbol{\tau}}_{f2} = J^{-1}\boldsymbol{\tau}_{\text{VOL}} + J^{-1}(1-d_g)\overline{\boldsymbol{\tau}}_g + J^{-1}(1-d_{f1})\overline{\boldsymbol{\tau}}_{f1} + J^{-1}(1-d_{f2})\overline{\boldsymbol{\tau}}_{f2} \quad (28)$$

with

$$\mathbb{P} = \mathbb{I} - \frac{1}{3}\boldsymbol{1}\otimes\boldsymbol{1}, \quad (29)$$

$$\boldsymbol{\tau}_{\text{VOL}} = Jp\boldsymbol{1};\quad \widetilde{\boldsymbol{\tau}}_g = \overline{\boldsymbol{F}}\widetilde{\boldsymbol{S}}_g\overline{\boldsymbol{F}}^{\mathsf{T}} = c\overline{\boldsymbol{b}}, \quad (30)$$

$$\widetilde{\boldsymbol{\tau}}_{f1} = \overline{\boldsymbol{F}}\widetilde{\boldsymbol{S}}_{f1}\overline{\boldsymbol{F}}^{\mathsf{T}} = 2k_{11}\overline{E}_1 e^{k_{21}\overline{E}_1^2}\underbrace{(\overline{\boldsymbol{a}}_1\otimes\overline{\boldsymbol{a}}_1)}_{\overline{\boldsymbol{h}}_1}, \quad (31)$$

$$\widetilde{\boldsymbol{\tau}}_{f2} = \overline{\boldsymbol{F}}\widetilde{\boldsymbol{S}}_{f2}\overline{\boldsymbol{F}}^{\mathsf{T}} = 2k_{12}\overline{E}_2 e^{k_{22}\overline{E}_2^2}\underbrace{(\overline{\boldsymbol{a}}_2\otimes\overline{\boldsymbol{a}}_2)}_{\overline{\boldsymbol{h}}_2}, \quad (32)$$

where $\mathbb{P}$ in this case is the Eulerian description of the deviatoric operator.

2.1.3. Ingredients of the damage model

We have assumed damage mechanisms are associated only with isochoric processes and therefore are independent from hydrostatic pressure. The internal dissipation has been obtained in Eq. (20) as:

$$\mathcal{D}_{\text{INT}} = \dot{d}_g\overline{W}_g + \dot{d}_{f1}\overline{W}_{f1} + \dot{d}_{f2}\overline{W}_{f2} \geqslant 0, \quad (33)$$

which allows us to define $\overline{W}_\alpha \geqslant 0$ as the thermodynamic variable conjugate to d_α, with $\alpha = \{g, f1, f2\}$. Non-negativeness of internal dissipation implies the damage variables to be non-decreasing, leading to the following condition:

$$d_\alpha \in [0,1],\quad \dot{d}_\alpha \geqslant 0 \quad \text{with } \alpha = \{g, f1, f2\}. \quad (34)$$

Following the model proposed by Simo (1987) and Simo and Ju (1987) we introduce for each phase the notion of equivalent strain $\bar{\tau}_\alpha$ as the following norm:

$$\bar{\tau}_\alpha = \sqrt{2\overline{W}_\alpha(\overline{\boldsymbol{C}})}. \quad (35)$$

We introduce also a set of damage surfaces $\Phi_\alpha = 0$, with $\alpha = \{g, f1, f2\}$, in the strain space that allows to define a set of damage criteria imposing, at any time $t \in \mathbb{R}^+$ of the loading process,

$$\Phi_g(\bar{I}_1, \bar{I}_2, r_g) = \sqrt{2\overline{W}_g} - r_g \leqslant 0, \quad (36)$$

$$\Phi_{f1}(\bar{I}_1, \bar{I}_4, r_{f1}) = \sqrt{2\overline{W}_{f1}} - r_{f1} \leqslant 0, \quad (37)$$

$$\Phi_{f2}(\bar{I}_1, \bar{I}_6, r_{f2}) = \sqrt{2\overline{W}_{f2}} - r_{f2} \leqslant 0. \quad (38)$$

Here r_α is the strain-like internal variable that defines the damage threshold at the current configuration satisfying $r_\alpha \geqslant r_\alpha^0$, with r_α^0 the initial damage threshold.

Eqs. (36)–(38) define the elastic domain of the material response. Damage evolution must satisfy the complementary Kuhn–Tucker loading/unloading conditions:

$$\dot{r}_\alpha \geqslant 0,\quad \Phi_\alpha \leqslant 0 \quad \text{and} \quad \dot{r}_\alpha\Phi_\alpha = 0; \quad (39)$$

as well as the damage consistency condition during persistent damage:

$$\dot{r}_\alpha\dot{\Phi}_\alpha = 0. \quad (40)$$

Denoting the normal to the damage surfaces $\boldsymbol{N}_\alpha := \partial\Phi_\alpha/\partial\overline{\boldsymbol{C}}$ the following alternative situations may occur: either

$$\Phi_\alpha < 0 \text{ or } \Phi_\alpha = 0 \quad \text{and} \quad \begin{cases} \boldsymbol{N}_\alpha : \delta\overline{\boldsymbol{C}} < 0, \\ \boldsymbol{N}_\alpha : \delta\overline{\boldsymbol{C}} = 0, \\ \boldsymbol{N}_\alpha : \delta\overline{\boldsymbol{C}} > 0. \end{cases} \quad (41)$$

where $\delta\overline{\boldsymbol{C}}$ stands for an admissible variation of the deviatoric strain tensor.

The model thus defined admits a closed integration of the rate of the internal variable r_α, being able to be integrated over time as:

$$r_\alpha(t) = \max_{\tau\in[0,t]}\left[r_\alpha^0, \sqrt{2\overline{W}_\alpha(\tau)}\right]. \tag{42}$$

We can also define a stress-like internal variable q_α whose rate of change is expressed with the following hardening rule (with $\alpha = \{g, f1, f2\}$):

$$\dot{q}_\alpha = H_\alpha(r_\alpha)\dot{r}_\alpha, \quad H_\alpha(r_\alpha) = \frac{\partial q_\alpha}{\partial r_\alpha}, \quad q_\alpha^0 = r_\alpha^0, \tag{43}$$

where H_α is the softening/hardening modulus, such that $H_\alpha(r_\alpha) > 0$ if there is strain hardening and $H_\alpha(r_\alpha) < 0$ if there is strain softening, and r_α^0 is the parameter that defines the initial size of the elastic domain. Damage parameters are finally expressed in terms of the previously introduced internal variables as:

$$d_g = 1 - \frac{q_g(r_g)}{r_g}, \quad d_{f1} = 1 - \frac{q_{f1}(r_{f1})}{r_{f1}}, \quad d_{f2} = 1 - \frac{q_{f2}(r_{f2})}{r_{f2}}. \tag{44}$$

2.1.4. Internal dissipation and softening regularisation

We can particularise the value of the internal dissipation given in expression (33), after some algebraic manipulations, as

$$\mathcal{D}_{\text{INT}} = \sum_{\alpha=g,f1,f2} \dot{d}_\alpha \overline{W}_\alpha = \sum_{\alpha=g,f1,f2} \frac{1}{2}(q_\alpha \dot{r}_\alpha - \dot{q}_\alpha r_\alpha), \tag{45}$$

where Eqs. (35) and (43) have been used.

We assume hereinafter our material undergoes strain softening. The rate of change of the stress-like internal variable $\dot{q}_\alpha$, with $\alpha = \{g, f1, f2\}$, can be defined as:

$$\dot{q}_\alpha = -H_\alpha(q_\alpha)\dot{r}_\alpha = -A_\alpha q_\alpha^\chi \dot{r}_\alpha, \tag{46}$$

where $-H_\alpha$ is the softening modulus, χ is a parameter that affects the rate of softening, and A_α is a value to be defined by imposing the objectivity of the approach regarding the characteristic size of the mesh in a finite element analysis (Wells and Sluys, 2000).

We reproduce damage in this work following the principles of the so called *smeared crack models* (Oh and Bazant, 1983) where inelastic phenomena are considered to be distributed inside the finite element. If our model has to be insensitive to the mesh size, the softening modulus H_α we use at each integration point has to be regularised (see Simo et al., 1993 for a full description) in terms of the material parameter *surface density of dissipation energy* and a characteristic size of the finite element (Oliver, 1989).

Let us define a subdomain $\Omega^h \in \mathcal{B}_0$ where inelastic processes take place. The volume of this subdomain, here we are assuming it is a finite element, can be defined as $\int_{\Omega^h} d\Omega = Sh$, where S is an averaged cross section and h is its characteristic size (see Fig. 1).

We assume there is a monotonic loading process and the material undergoes strain softening, so the total dissipated energy W_{TOT} until material exhaustion is:

$$\begin{aligned} W_{\text{TOT}} &= \int_{\Omega^h} d\Omega \left(\int_{t=t_d}^{\infty} \mathcal{D}_{\text{INT}} dt \right) \\ &= \int_{\Omega^h} d\Omega \left(\int_{t=t_d}^{\infty} \sum_{\alpha=g,f1,f2} \frac{1}{2}(q_\alpha \dot{r}_\alpha - \dot{q}_\alpha r_\alpha) dt \right) \\ &= \sum_{\alpha=g,f1,f2} \int_{\Omega^h} d\Omega \left(\int_{t=t_d}^{\infty} \frac{1}{2}(q_\alpha \dot{r}_\alpha - \dot{q}_\alpha r_\alpha) dt \right). \end{aligned} \tag{47}$$

If we impose, for each phase $\alpha = \{g, f1, f2\}$, that the total dissipated energy is given by the material parameter *surface density of dissipated energy* G_α^f, after some algebraic manipulations in Eq. (47) and using expression (46) we arrive to:

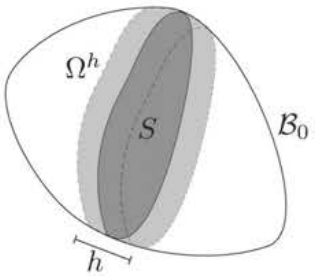

Fig. 1. Damaged band Ω^h in a continuum domain.

$$\begin{aligned} W_{\text{TOT}} &= \sum_{\alpha=g,f1,f2} \int_{\Omega^h} d\Omega \left[\frac{1}{A_\alpha} \frac{(q_\alpha^0)^{2-\chi}}{(2-\chi)} \right] \\ &= \sum_{\alpha=g,f1,f2} Sh \left[\frac{1}{A_\alpha} \frac{(q_\alpha^0)^{2-\chi}}{(2-\chi)} \right] = \sum_{\alpha=g,f1,f2} SG_\alpha^f, \end{aligned} \tag{48}$$

which allows us to obtain the expression for A_α in Eq. (46) as:

$$A_\alpha = \frac{(q_\alpha^0)^{2-\chi}}{(2-\chi)} \frac{1}{G_\alpha^f} h. \tag{49}$$

Finally, we obtain the regularised softening modulus as

$$H_\alpha(q_\alpha(t), h) = -\frac{(q_\alpha^0)^{2-\chi}}{(2-\chi)} \frac{1}{G_\alpha^f} q_\alpha^\chi(t) h, \tag{50}$$

where h, in case the domain has been discretised by finite elements, is the characteristic length of this element (Oliver, 1989).

2.1.5. Summary of material parameters

In this model, for each material phase $\alpha = \{g, f1, f2\}$ we need to characterise the effective strain energy function $\overline{W}_\alpha$, the initial size of the elastic domain r_α^0, the surface density of dissipated energy G_α^f and the rate of softening χ. The total amount of material parameters needed is summarised in Table 1.

2.2. Mesoscopic characterisation of fibre inelastic behaviour

In this study we derive the macroscopic material parameters $\{k_{1i}, k_{2i}, \sigma_\gamma^{fi}, \mathcal{G}_{fi}^f\}$ for the family of fibres i from the mechanical properties of its mesoscopic constituents. We have assumed a simplified hierarchical structure of soft tissues such that we consider soft tissues as a fibre reinforced composite and fibres as a fibril reinforced composite. Fibrils, assumed as a staggered array of tropocollagen molecules, is the smallest scale we have considered (see Fig. 2).

This section is summarised as follows. Firstly, we obtain the fibril elastic stretch threshold considering that its reference configuration has a wavy arrangement. Afterwards we study the mesomechanical behaviour of the fibril: we introduce the two-dimensional Hodge–Petruska model (Petruska and Hodge, 1964), we define the mechanical features of each component of the fibril and we characterise the elastic/inelastic mesomechanical behaviour of the fibril as a whole. Finally, we obtain the macromechanical behaviour of the fibres by homogenising the properties of the fibrils and the proteoglycan-rich ground matrix.

2.2.1. Fibril mesoscopic model

2.2.1.1. Fibril elastic stretch threshold. The wavy structure of the fibrils has an important bearing on the mechanical properties of soft tissues. It affects both the evolution of the tension stiffening displayed in the uniaxial tension test and the value of the elastic stretch threshold (assuming the crimped configuration of the fibril

Table 1
Material parameters.

Component	Elastic behaviour		Inelastic behaviour	
Ground matrix	c (Pa)	Shear modulus	σ_Y^g (Pa)	Stress elastic threshold in the uniaxial homogeneous tension test
			$\mathcal{G}_g^f$ (N/m)	Surface density of dissipated energy
			χ_g (–)	Rate of softening
Family i of fibres $i = \{1,2\}$	k_{1i} (Pa)	Elastic constant	σ_Y^{fi} (Pa)	Stress elastic threshold in the uniaxial homogeneous tension test
	k_{2i} (–)	Elastic constant	$\mathcal{G}_{fi}^f$ (N/m)	Surface density of dissipated energy
			χ_{fi} (–)	Rate of softening
Tissue	K (Pa)	Bulk modulus		–

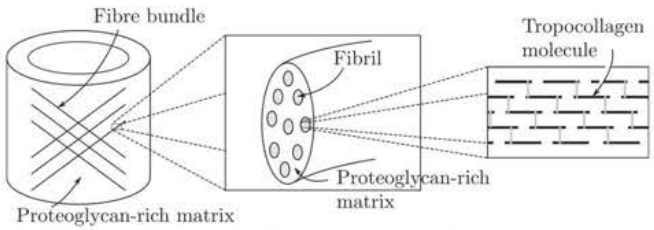

Fig. 2. Hierarchical structure of soft tissues.

is its reference configuration). We consider a crimped fibril displaying a sinusoidal shape (Fung, 1993) characterised by the dimensionless parameter r (see Fig. 3).

The total length L can be expressed as:

$$L = \frac{2\alpha}{\pi}\sqrt{1+\pi^2 r^2}\,\underbrace{\mathrm{E}\left(\frac{\pi^2 r^2}{1+\pi^2 r^2}\right)}_{E(m)}, \tag{51}$$

where $\mathrm{E}(m)$ is the complete elliptic integral of the second kind. We assume as a hypothesis that (a) *the onset of damage occurs when the fibril is fully stretched* (Meyers et al., 2008) and (b) *both fibril and fibre share the same elastic stretch threshold* λ_e. In this case we obtain the elastic threshold of the stretch for the fibres as:

$$\lambda_e = \frac{L}{\alpha} = \frac{2}{\pi}\sqrt{1+\pi^2 r^2}\,\mathrm{E}\left(\frac{\pi^2 r^2}{1+\pi^2 r^2}\right) \tag{52}$$

whose dependence $\lambda_e = \lambda_e(r)$ is described in Fig. 4.

2.2.1.2. The two dimensional Hodge–Petruska model. Following (Buehler, 2008 and Tang et al., 2010), a two dimensional Hodge–Petruska arrangement (Petruska and Hodge, 1964) has been considered to reproduce the staggered structure of the tropocollagen molecules inside a fibril. In this model, see Fig. 5, tropocollagen molecules (TC) are considered as only-tension bearing line elements displaying a staggered structure. The length l of each TC molecule is around 300 nm and its diameter d is around 1.5 nm, the distance h of stagger is around 67 nm and the gap s between the ends of successive molecules is around 40 nm (Fung, 1993). Finally, distance D stands for the equilibrium distance between tropocollagen molecules, which has been considered as equal to the microfibril size of 4–20 nm measured in Ottani et al. (2001).

Intermolecular adhesion, and therefore geometrical stability of the structure, is accomplished by the presence of (a) intermolecular distributed adhesive forces along the TC molecules and (b) localised cross-links at their ends (Bailey and Sims, 1976; Buehler, 2006a). The intermolecular adhesive forces are distributed along the overlapped TC molecular length χl and the localised cross links along $\eta = 60$ Å at the end of the TC molecules (Buehler, 2006a). These cohesive forces between TC molecules and the intermolecular bonds within them provides the inner response against an external solicitation. Table 2 summarises the proposed geometrical parameters of the Hodge–Petruska model used in this work.

2.2.1.3. Fibril mesomechanical model in elastic regimen. We assume as a hypothesis that when a fibril is subjected to axial tension all TC molecules are loaded uniformly. The individual behaviour of each TC molecule can be simplified according to the scheme displayed in Fig. 6. In this model the stress supported by the TC molecule is transmitted to adjacent molecules through (a) the distributed unions along the overlapped molecular length and (b) the localised cross-links at its end.

Under quasi-static conditions, the tension in the TC molecule must be balanced by the strength provided in the distributed

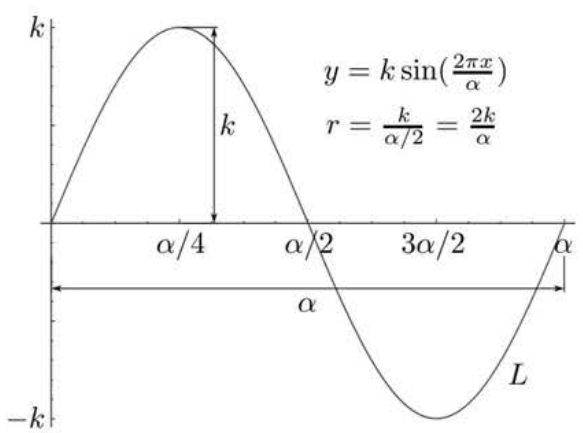

Fig. 3. 1-D model of a wavy fibril.

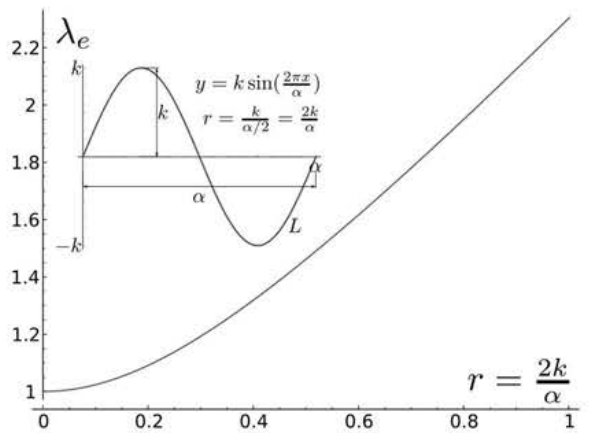

Fig. 4. Dependence $\lambda_e = \lambda_e(r)$.

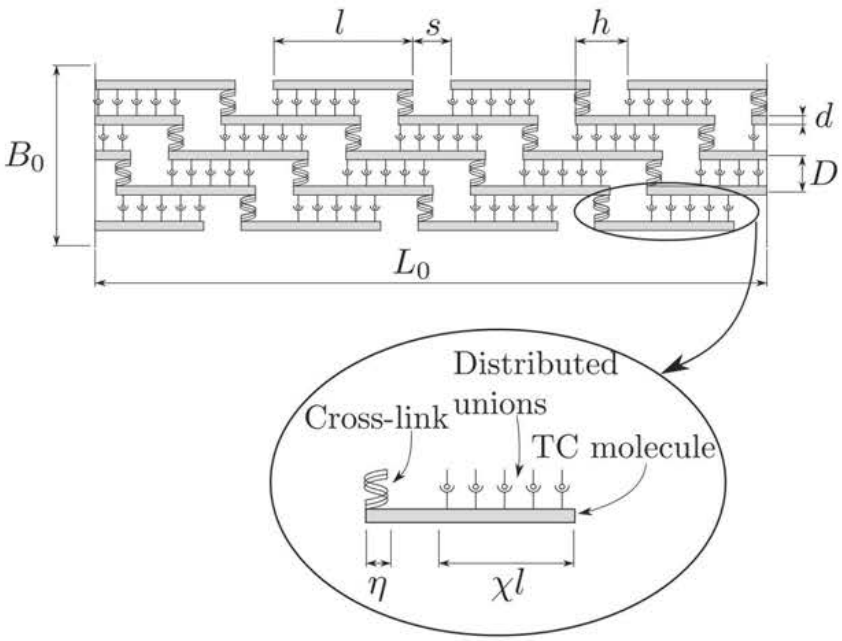

Fig. 5. 2-D Hodge–Petruska model.

unions and in the cross-links (see Fig. 6). This scheme of forces can be interpreted as a series arrangement of the TC molecule with a parallel arrangement of the unions between TC molecules (see Fig. 7(a)).

We need to characterise the mesomechanical behaviour of each of the ingredients included in the model (TC molecule, distributed unions and cross-links). If we assume a mesoscopic linear behaviour, we have to define for each ingredient only three of the parameters shown in Fig. 7(b). Table 3 summarises the reference values of the parameters *elastic stiffness*, *ultimate strength* and *dissipated energy* used in this work. Here we have considered the dissipated energy as the work required to exhaust the bearing capacity of the element.

2.2.1.4. Fibril failure modes. We associate the onset of inelastic processes in the tissue with the beginning of degradation in the fibril components. If we study the mechanical idealisation of the TC molecule shown in Fig. 6, loss of bearing capacity can be related either with the failure of the collagen chains or with the failure of the adherent unions between TC molecules. Due to the high tensile strength of the collagen chains (Ottani et al., 2001) we assume structural failure is associated only with the loss of cohesion at the unions between TC molecules.

In this work we propose as a hypothesis that there are two possible failure mechanisms associated with the loss of cohesion at

Table 2
Geometrical properties of fibril components.

Description	Symbol	Value
Waviness parameter	r	0.33
TC molecular length	l	300 nm[a]
TC molecular diameter	d	1.5 nm[a]
Gap between TC molecules	s	40 nm[a]
Distance of stagger	h	67 nm[b]
Equilibrium distance between TC molecules	D	8 nm[c]
Cross-link concentration length	η	6 nm[d]

[a] Bhattacharjee and Bansal (2005).
[b] Liao et al. (2005).
[c] Microfibril size of 4–20 nm in Ottani et al. (2001).
[d] Buehler (2008).

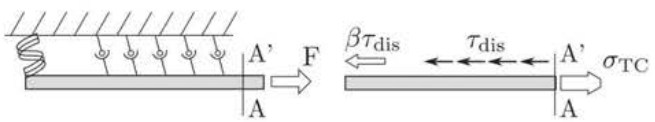

Fig. 6. Unidimensional equilibrium of the TC molecule.

the unions between TC molecules. Failure mechanisms depend on the relationship between the maximum cohesion strength $\eta\beta\tau^u_{dis}$ provided by the cross-links and the maximum cohesion strength $\chi l\tau^u_{dis}$ provided by the distributed unions. If the cross-links provide a greater cohesion strength, a plane of weakness will appear along the distributed unions (failure mode 1), and if otherwise, a plane of weakness will appear along the cross-links (failure mode 2). Fig. 8 displays both planes of weakness, which form the following angles with the fibril axis direction (see Fig. 5 for the geometrical parameters):

$$\tan\theta_1 = \frac{D}{l-h+s}; \qquad \tan\theta_2 = \frac{D}{h}. \tag{53}$$

We define now a critical length l_{cr} as the minimum length of the TC molecule such that the maximum strength of the cross-links equals the maximum strength of the distributed unions:

$$l_{cr} = \frac{\eta\beta\tau^u_{dis}}{\chi\tau^u_{dis}} = \frac{\eta\beta}{\chi}. \tag{54}$$

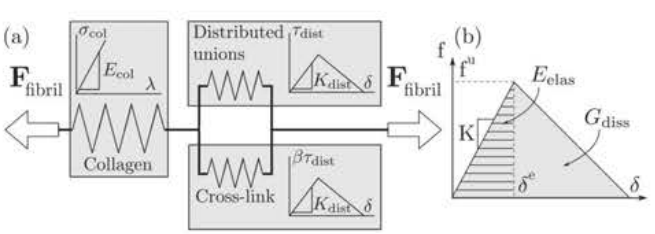

Fig. 7. (a) Idealised mechanical model. (b) Mechanical characterisation of individual components.

Table 3
Mesomechanical properties of fibril components.

Component	Elastic stiffness	Ultimate strength	Dissipated energy (N m)
TC molecule	$E_{col} = 50.0$ pN/Å^2[a]	$\sigma^u = 10.0$ pN/Å^2[b]	–
Distributed unions	$K_{dist} = 1.18$ nN/Å[c]	$\tau^u_{dist} = 5.55$ pN/Å[d]	$G_{dist} = \frac{1}{2}\tau^u_{dist}(\chi l)^2$[e]
Cross-links	$K_{dist} = 1.18$ nN/Å[c]	$\tau^u_{c\text{-}l} = \beta\tau^u_{dist} = 69$ pN/Å[f]	$G_{c\text{-}l} = \frac{1}{2}\tau^u_{c\text{-}l}\eta^2$[g]

[a] Collagen Young's modulus from Lorenzo and Caffarena (2005).
[b] Collagen tensile strength from Ottani et al. (2001).
[c] Intermolecular tensile stiffness parameter from Buehler (2008).
[d] Interaction between two TC molecules without cross-links from Buehler (2006a).
[e] Total dissipated energy in distributed unions along the overlapped TC molecular length.
[f] Cross-link strength for $\beta = 12.5$ when one cross-link is present at each end of a TC molecule as proposed by Buehler (2008).
[g] Total dissipated energy in cross-links along η at the end of the TC molecule.

This parameter l_{cr} gives us a criterion to identify which is the dominant failure mode in the fibril such that:

$$\text{If} \quad l < l_{cr} \longrightarrow \text{Failure mode 1}, \tag{55}$$

$$\text{If} \quad l > l_{cr} \longrightarrow \text{Failure mode 2}. \tag{56}$$

2.2.1.5. Fibril inelastic behaviour mesomechanical characterisation. The onset and development of each of the previous failure modes affect the maximum tension of the fibril in elastic regime and the total amount of available dissipation energy. We describe now the mechanical characterisation for both failure modes and we derive afterwards the overall behaviour of the fibril, assuming that the length of the TC molecules inside the fibril follows a normal distribution.

Failure mode 1 is associated with the decohesion of the distributed unions between TC molecules. The maximum stress *per unit area of the fibril* is therefore:

$$\sigma^{\text{u-mode 1}}_{\text{fibril}} = \frac{\chi l \tau^u_{dis}}{D^2}, \tag{57}$$

where D stands for the equilibrium distance between tropocollagen molecules, and the surface density of dissipated energy per unit area of the fibril is:

$$\mathcal{G}^{\text{mode 1}}_{\text{fibril}} = \frac{1}{2}\tau^u_{dis}(\chi l)^2\frac{1}{D^2}. \tag{58}$$

Failure mode 2 is associated with the decohesion of the cross-links forces between the ends of TC molecules. In this case the maximum stress per unit area of the fibril is:

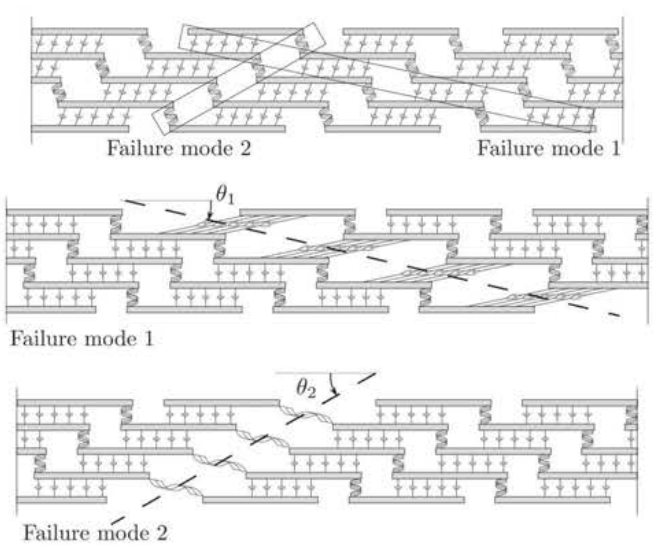

Fig. 8. Fibril failure models.

$$\sigma^{\text{u-mode 2}}_{\text{fibril}} = \frac{\eta\beta\tau^u_{dis}}{D^2}, \tag{59}$$

and the surface density of dissipated energy per unit area of the fibril is:

$$\mathcal{G}^{\text{mode 2}}_{\text{fibril}} = \frac{1}{2}\beta\tau^u_{dis}\eta^2\frac{1}{D^2}. \tag{60}$$

The characteristic length l_{cr} defined in Eq. (54) allows us to discriminate which failure mode will take place in the fibril. Assuming the lengths of the TC molecules inside a fibril have a normal distribution (characterised by a mean length l_m and a variance σ, see Fig. 9), we can define the proportion of mode 1 failures inside a fibril as:

$$D_1 = \frac{1}{2}\left[1 + \text{erf}\left(\frac{l_{cr} - l_m}{\sigma\sqrt{2}}\right)\right]. \tag{61}$$

Eqs. (57)–(61) give us finally the first two expressions that characterise the fibril mechanical behaviour in the mesoscopic scale:

$$\sigma^{u}_{\text{fibril}} = D_1\sigma^{\text{u-mode 1}}_{\text{fibril}} + (1 - D_1)\sigma^{\text{u-mode 2}}_{\text{fibril}} \tag{62}$$

$$\mathcal{G}_{\text{fibril}} = D_1\mathcal{G}^{\text{mode 1}}_{\text{fibril}} + (1 - D_1)\mathcal{G}^{\text{mode 2}}_{\text{fibril}}, \tag{63}$$

where we have considered that the overall behaviour of the fibril is the weighted average of the behaviours of modes 1 and 2.

The stored elastic energy density *per unit volume of the fibril* at the onset of damage has two components: the stored elastic energy in the TC molecule and the stored elastic energy in the intermolecular adhesion unions (see Fig. 6). Both the TC molecule and the intermolecular adhesion unions undergo the same level of internal force (owing to the series arrangement):

$$f^u_{fibril} = \sigma^{u}_{\text{fibril}}D^2. \tag{64}$$

Assuming linear elastic behaviour for each component, and using the elastic stiffness E_{col} and K_{dist} for the collagen and the intermolecular adhesion unions, we can obtain the elastic energy stored in the TC molecule as (see Fig. 6):

$$w^0_{\text{TC molecule}} = \frac{1}{2}f^u_{fibril}\frac{f^u_{fibril}(1 - \chi)l}{E_{col}d^2} \tag{65}$$

and the elastic energy stored in the intermolecular adhesion unions as:

$$w^0_{\text{dist unions}} = \frac{1}{2}f^u_{fibril}\frac{f^u_{fibril}}{K_{dist}}. \tag{66}$$

Expressions (65) and (66) give us finally an elastic energy density *per unit volume of the fibril*:

$$W^0_{\text{fibril}} = \frac{1}{lD^2}\left(w^0_{\text{TC molecule}} + w^0_{\text{dist unions}}\right). \tag{67}$$

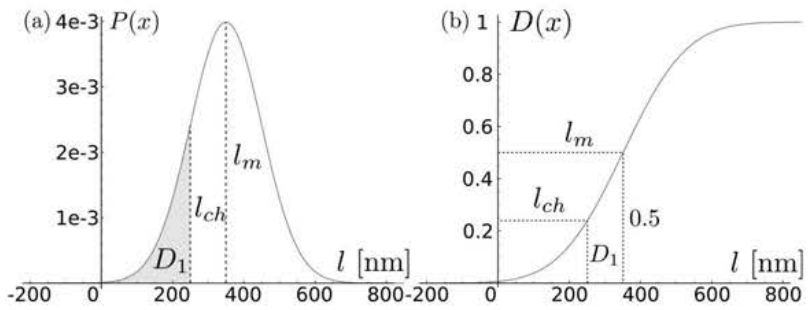

Fig. 9. Probabilistic distribution of the TC molecular length.

The values derived in Eqs. (62), (63) and (67) allows us to characterise the mechanical behaviour of the fibril in the mesoscopic scale using the mechanical properties of its basic components.

2.2.2. Fibre macromechanical characterisation

We assume fibrils are aligned with the fibre axis and fibres of the same family share a common mean direction inside the tissue. We also consider the fibre and the tissue as homogenised continua (the fibre as a fibril reinforced composite and the tissue as a fibre reinforced composite). This approach allows us to define the homogenised properties of each composite as functions of the mechanical properties of the constituents and its volume fractions.

In this section we firstly obtain the mesoscopic properties of the fibre. To do so, we define the volume fractions of the fibrils and the ground matrix in terms of its relative thicknesses inside the fibre. Afterwards, we obtain the macroscopic properties of the fibre in terms of the volume fraction of the fibre inside the tissue. Finally we calculate, for each family of fibres, the material parameters of the continuum damage model introduced in Section 2.1 (see parameters in Eqs. (16) and (49)). We impose that the inelastic properties of this model, *i.e.* the uniaxial stretch and stress elastic thresholds, the stored elastic energy that defines the initial elastic domain and the surface density of dissipated energy, are given by the macroscopic values derived in the upscaling homogenisation process.

2.2.2.1. Fibre mesomechanical model. Fibres can be considered as a bundle of closely packed thin fibrils linked by very thin proteoglycan filaments (GAGs). Proteoglycans determine the distance of two neighbouring fibrils to fasten themselves into a bundle (Ushiki, 2002). In this work we consider a fibre two-dimensional model characterised only by the fibril diameter B_0 and the interfibrillar distance B_1 (see Fig. 10(a)). We assume also there is a compatibility of strains for both the fibril and the proteoglycan-rich ground matrix phases. Following these assumptions the mechanical properties of the fibre at mesoscale level are:

$$\sigma^{\mathrm{u}}_{\mathrm{fibre}} = \frac{B_0}{B_0+B_1}\sigma^{\mathrm{u}}_{\mathrm{fibril}} + \frac{B_1}{B_0+B_1}\sigma^{\mathrm{u}}_{\mathrm{GAG}} \approx \frac{B_0}{B_0+B_1}\sigma^{\mathrm{u}}_{\mathrm{fibril}}, \tag{68}$$

$$W^0_{\mathrm{fibre}} = \frac{B_0}{B_0+B_1}W^0_{\mathrm{fibril}} + \frac{B_1}{B_0+B_1}W^0_{\mathrm{GAG}} \approx \frac{B_0}{B_0+B_1}W^0_{\mathrm{fibril}}, \tag{69}$$

$$\mathcal{G}_{\mathrm{fibre}} = \frac{B_0}{B_0+B_1}\mathcal{G}_{\mathrm{fibril}} + \frac{B_0}{B_0+B_1}\mathcal{G}_{\mathrm{GAG}}, \tag{70}$$

where we have assumed that (a) the proteoglycan-rich matrix and the fibril have a parallel arrangement (see Fig. 10(b)) and (b) the elastic stiffness of the GAGs molecules is so low that we they do not contribute to the yield stress and the stored elastic energy of the fibre. However, the ductile rupture of the GAGs molecules do provide surface density of dissipation energy.

Table 4 summarises the mechanical and geometrical properties of the fibre two-dimensional model used in Eqs. (68)–(70).

2.2.2.2. Fibre macroscopic elastic energy density function. At macroscopic scale we have modelled soft tissues as composites formed by an incompressible ground matrix and one or several families of fibres. Fibres are represented in the composite by a volumetric

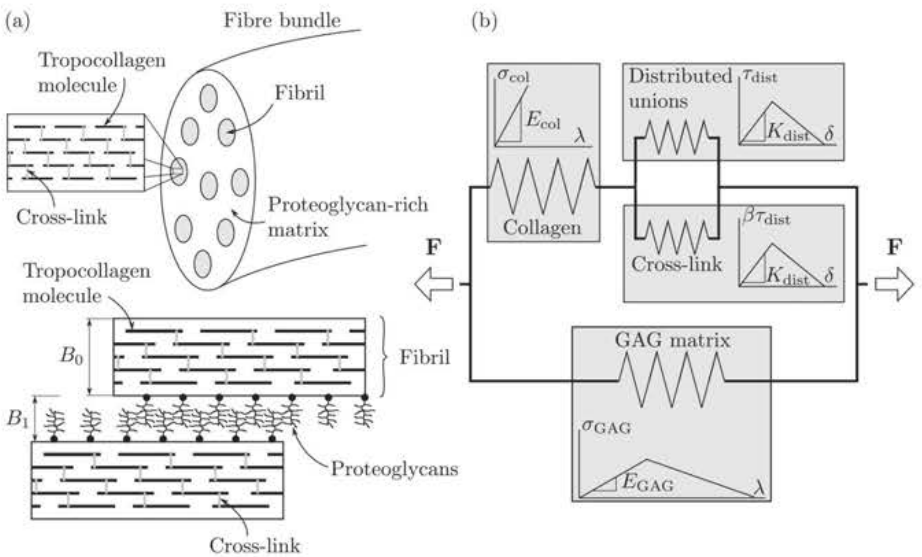

Fig. 10. 2-D fibre model.

Table 4
Properties of fibre components.

Component	Symbol	Value
GAG's molecules surface density of dissipation energy	$\mathcal{G}_{GAG}$	10^3 pN/Å
Fibril width	B_0	180 nm
Proteoglycan-rich matrix width	B_1	100 nm
Fibre volume fraction in the tissue	v^f	0.22[a]

[a] See Fig. 4 in Driessen et al. (2003).

fraction v^f and therefore the stresses and energy densities of Eqs. (68)–(70) must be homogenised in order to obtain the macroscopic values of the fibre at tissue level. Macroscopic expressions of the mechanical properties of the fibres are thus obtained as:

$$\sigma_{\text{fibre}}^{\text{u-tissue}} = v^f \sigma_{\text{fibre}}^{\text{u}}, \tag{71}$$

$$W_{\text{fibre}}^{0-\text{tissue}} = v^f W_{\text{fibre}}^{0}, \tag{72}$$

$$\mathcal{G}_{\text{fibre}}^{\text{tissue}} = v^f \mathcal{G}_{\text{fibre}}, \tag{73}$$

where v^f is the fibre volume fraction in the tissue. Mechanical properties of the incompressible ground matrix depend on the properties of the GAGs molecules. It is commonly accepted that this material can be modelled at the macroscopic scale with a neo-Hookean law (Holzapfel et al., 2000).

The values of $\sigma_{\text{fibre}}^{\text{u-tissue}}$ and $W_{\text{fibre}}^{0\text{-tissue}}$ given in equations (71) and (72), along with the uniaxial elastic stretch threshold λ_e given in Eq. (52), allow us to fully characterise the macroscopic constitutive model for the families of fibres. To achieve that we impose, in the uniaxial traction test and at the onset of damage, that the yield stress and the stored elastic energy density given by the constitutive model match the values of equations (71) and (72) (see Fig. 11).

The fibre effective strain energy function defined in Eq. (16), particularised for the uniaxial traction test when the fibre is aligned with the direction of stretching is:

$$\overline{\Psi}^{\text{fibre}} = \frac{k_1}{2k_2}\left(e^{k_2(\lambda^2-1)^2} - 1\right), \tag{74}$$

where k_1 and k_2 are two material parameters to be determined and λ is the stretch in the fibre axial direction. The fibre uniaxial stress is therefore:

$$\sigma^{\text{fibre}} = \lambda \frac{\partial \overline{\Psi}^{\text{fibre}}}{\partial \lambda} = 2k_1(\lambda^4 - \lambda^2)e^{k_2(\lambda^2-1)^2}. \tag{75}$$

Eqs. (74) and (75) allow us to finally obtain k_1 and k_2 as the solution of the following system of nonlinear equations:

$$\sigma^{\text{fibre}}(\lambda_e) = 2k_1(\lambda_e^4 - \lambda_e^2)e^{k_2(\lambda_e^2-1)^2} = \sigma_{\text{fibre}}^{\text{u-tissue}}, \tag{76}$$

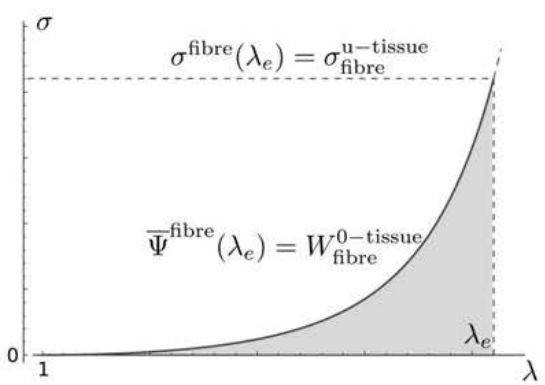

Fig. 11. Uniaxial fibre model.

$$\overline{\Psi}^{\text{fibre}}(\lambda_e) = \frac{k_1}{2k_2}\left(e^{k_2(\lambda_e^2-1)^2} - 1\right) = W_{\text{fibre}}^{0-\text{tissue}}, \tag{77}$$

where the values of $\sigma_{\text{fibre}}^{\text{u-tissue}}$ and $W_{\text{fibre}}^{0\text{-tissue}}$ are given in Eqs. (71) and (72). The nonlinear equation system (76) and (77) has been numerically solved by using the `optimize` package of `scipy` library (Jones et al., 2001).

3. Results

In this section we have performed mechanical analysis at fibril, fibre and tissue levels. Our aim is to study the behaviour of the model at each of the hierarchical scales we have considered. Unless otherwise specified, the values of the mesoscopic parameters used to characterise the tissue are given in Tables 2–4.

3.1. Fibril behaviour analysis

Firstly, we analyse how the cohesive force of the cross-links (defined as a function of parameter β, see Table 3) affects the yield strength of the fibril. The influence of β parameter appears only when the material failure is associated with the breakage of cross-links (failure mode 2). In Fig. 12(a) we plot the stress level $\sigma_{\text{fibril}}^{u}$ of the fibril at the onset of damage, see Eq. (62), as a function of parameter β. We see an increase in the yield strength with increasing the bearing capacity of the cross-links, until the strength of the cross-links is so large that failure occurs along the distributed unions in the overlapped length (failure mode 1). In Fig. 12(a) we compare our results with those presented in Buehler (2008), where molecular dynamics (MD) simulations were made using a short chain of collagen molecules. Further MD simulations were performed in Tang et al. (2010) increasing the size of the collagen fibril until it behaved as a representative volume element. Results presented in Tang et al. (2010) show a subtle increase in the yield strength (see Fig. 4 in Tang et al., 2010) if we compare with those presented previously in Buehler (2008).

We study also how the length of the TC molecule affects the yield strength of the fibril when, in this case, material failure is associated with the breakage of the distributed unions along the overlapped length (failure mode 1). In Fig. 12(b) we see that there is an increase of the yield strength when we increase the length of the TC molecule, until it reaches a threshold value at which the failure occurs through the cross-links (failure mode 2).

Experimental tests of individual fibrils can be found in Shen et al. (2008, 2010). In these studies, the first deviation from linearity occurred at a yield strength of 0.22 ± 0.14 GPa (nominal stress). Our model predicts a stronger response of fibrils in case cross-links are present. In the authors' opinion, more research should be made to characterise the mechanical behaviour of the constituent elements of the fibril, in particular the mechanical interaction between two TC molecules along their overlapped length. Following Buehler (2006a), we have considered in this work an ultimate strength of the distributed unions of $\tau_{\text{dist}}^{u} = 5.55$ pN/Å, which is also used to calculate the ultimate strength of the cross-links as $\tau_{\text{c-l}}^{u} = \beta\tau_{\text{dist}}^{u}$. In order to better approximate the experimental results presented in Shen et al. (2008, 2010), a smaller value of parameter τ_{dist}^{u} should be used.

3.2. Fibre behaviour analysis

We use the homogeneous simple tensile test to analyse the behaviour of the fibres. The test specimen is a parallelepiped with dimensions $a = 2.81$ mm, $b = 0.32$ mm and $h = 12.5$ mm (see Fig. 13(a)). The matrix of the composite is assumed to have null strength and the fibres are oriented in the direction of stretching. In this section we perform a sensitivity analysis of the following

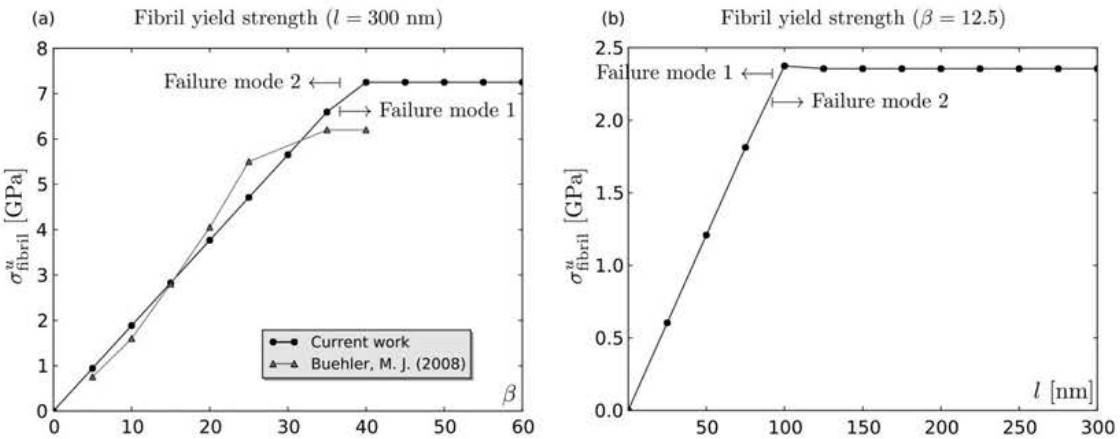

Fig. 12. (a) TC molecule yield strength as a function of cross-link β parameter. (b) TC molecule yield strength as a function of the length of the TC molecule.

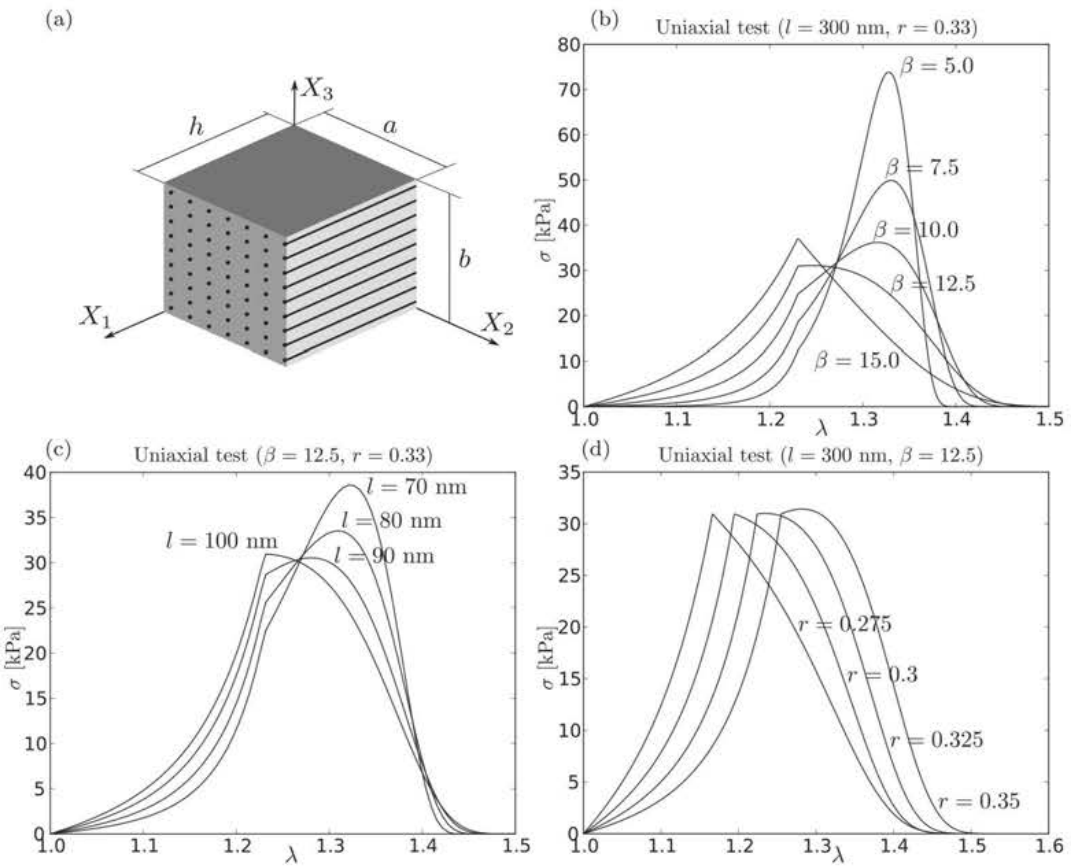

Fig. 13. Fibre behaviour analysis.

parameters: the cross-link strength (Fig. 13(b)), the TC molecular length (Fig. 13(b)), and the waviness parameter (Fig. 13(d)). These stress-stretch curves present tension-stiffening in the elastic domain associated with the fibril recruitment along the stretching direction. The onset of inelastic processes in the fibre is associated with a discontinuity (a kink) in the slope of the curves stress-stretch. After that point, the regularised damage model of Section 2.1 requires the total dissipated energy to be given by the material parameter *surface density of dissipated energy*, defined in Eq. (70). Therefore, the shape of the softening branch of the curves depends on the size (the length h in Fig. 13(a)) of the domain, *i.e.*, the larger the length h the brittler the inelastic behaviour.

We firstly investigate the influence of the cross-link strength (β parameter) on the fibre stress-stretch response. In Fig. 13(b) we compare the stress-stretch behaviour for different values of β. As we can see the yield strength and the brittleness of the model increase with increasing β. We find a similar behaviour when we increase the length of the TC molecule. In Fig. 13(c) we show the stress-stretch responses for different values of l_{m}. When we increase the value of the TC molecular length, we obtain an

increasing value of the yield strength and a slight increase of the brittle behaviour (see the different vertical scales in Fig. 13(b) and (c)). We finally study the fibre behaviour when the fibril waviness is modified. In Fig. 13(d) we plot the stress–stretch curves when the waviness parameter r is increased. We appreciate that when we increase the value of r the elastic stretch threshold is increased and a small decrement of the brittleness takes place.

3.3. Soft tissue behaviour analysis

Mesoscopic values of Tables 2–4 give us the derived macroscopic fibre material parameters at tissue level summarised in Table 5.

Several works have been published with numerical fitting of material parameters $\{k_1, k_2\}$ to the elastic physiological response of fibred soft tissues (see Sommer and Holzapfel, 2012; Weisbecker et al., 2012 or Pierce et al., 2015 among others). In Weisbecker et al. (2012), range values of $\{k_1 = [240, 940]$ kPa, $k_2 = [5.790, 34.79]\}$ are given for healthy thoracic aorta and $\{k_1 = [2580, 10500]$ kPa, $k_2 = [0.00, 32.4]\}$ for healthy abdominal aorta. However, these values are not exactly comparable with those of Table 5 because these works have used an extended version of Eq. (16) taking into account the dispersion in the collagen fibre directions (see Gasser et al., 2006 for more details).

Experimental data about failure properties of soft tissues can be found in literature although these values present some variability. Material parameters associated with fracture of soft tissues are associated to different types of tests: tensile, inflation, tearing, splitting, and peeling tests (see Sommer et al., 2008 and references therein). If we restrain ourselves to the aortic tissue, we find values of the axial strength from 1.21 ± 0.33 MPa in human abdominal aorta (Vorp et al., 1996) to 1.95 ± 0.60 MPa in human descending thoracic aorta (Adham et al., 1996). The mesoscopic parameters chosen in our model lead to a value (6.81 MPa) larger than the experimental axial strength found in aortic tissues. One possible cause of this discrepancy could be our overestimation of the tensile strength of the fibril that has already been discussed in Section 3.1. There is also uncertainty in the value of the dissipated energy of collagenous fibres in soft tissues in the extension test. We find that the value of dissipated energy in the aortic tissue in the splitting test range from 1.7 N/m in human thoracic and abdominal aorta (Tiessen and Roach, 1993) to 159 ± 9 N/m in porcine descending thoracic aorta (Carson and Roach, 1990). When we compare these values with the one presented in Table 5 we must bear in mind that the failure modes considered are different (extension *vs.* splitting).

In this section we study the deformation of a square plate with a hole (see Fig. 14(a)) when it is stretched in a tensile test. An increasing displacement is imposed along the X_1 direction at sections A and A′ while the remaining displacement degrees of freedom are set to zero. The study has mirror symmetry so we discretise only one eighth of the model (the domain placed in the first octant). We use three geometrical discretisations, called *Mesh1*, *Mesh2* and *Mesh3*, with different characteristic element lengths, see Table 6 and Figs. 14(b)–(d)).

Table 5
Macroscopic fibre material parameters.

Symbol	Value	Units	Equation
k_1	1704.3	(kN/m^2)	(76) and (77)
k_2	3.585	(–)	(76) and (77)
σ_u	6.81	(MN/m^2)	(71)
$\mathcal{G}_f$	1.38	(N/m)	(73)

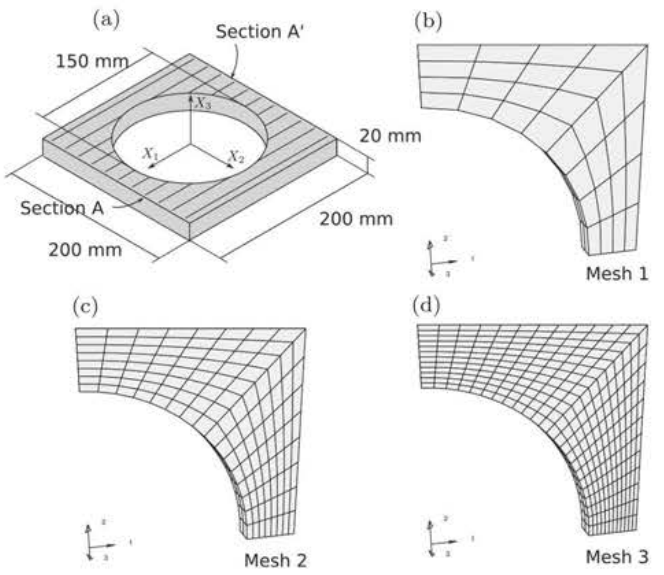

Fig. 14. (a) Description of the model. (b) Geometrical discretisation *Mesh1*. (c) Geometrical discretisation *Mesh2*. (d) Geometrical discretisation *Mesh3*.

Table 6
Mesh geometric properties.

Name	Elements	Type	Characteristic length h (mm)
Mesh1	64	8-node brick	25.0
Mesh2	256	8-node brick	12.5
Mesh3	576	8-node brick	8.33

Only one family of fibres is considered. This family is oriented in the X_1 direction, so its orientation vector at the reference configuration is $\mathbf{a}_0 = (1, 0, 0)$. We characterise the mechanical behaviour of the fibres with the material parameters summarised in Table 5. These fibre parameters were obtained from mesoscopic values in Tables 2–4. Ground matrix behaviour is reproduced by using a fully elastic neo-Hookean model with shear modulus $c = 5$ MN/m^2.

In this displacement-controlled tension test we increase monotonically the prescribed displacement from zero up to a maximum value of 56.3 mm. In Fig. 15(a) we show the force-stretch response of the model. The two solid black curves represent the fully elastic response of the composite (upper) and the isotropic elastic neo-Hookean matrix (lower). Discontinuous lines represent the force-stretch response for the discretisations *Mesh1*, *Mesh2* and *Mesh3*. We can identify the onset of damage around the stretch value $\lambda = 1.15$, when the equilibrium curves of the damaged composite separate from the fully elastic behaviour. The equilibrium curves obtained with the three geometrical discretisations are quite similar due to the softening regularisation explained in Section 2.1.4.

Although this model enforces the mesh-objectivity of the structural response two difficulties emerge: the definition of the correct characteristic length for each finite element used in Eq. (50) and the influence of the mesh bias on the numerical results. The first problem is solved by defining an approximate characteristic length as the size of the element in the stretching direction (see Table 6). In Fig. 15(b)–(d) the contours of the damage function are plotted for the three geometrical discretisations. As we can see, damage is more pronounced around the tip of the hole where the resistant section is smaller and where we find the highest values of the stresses. The domain completely damaged in the three numerical simulations is almost the same.

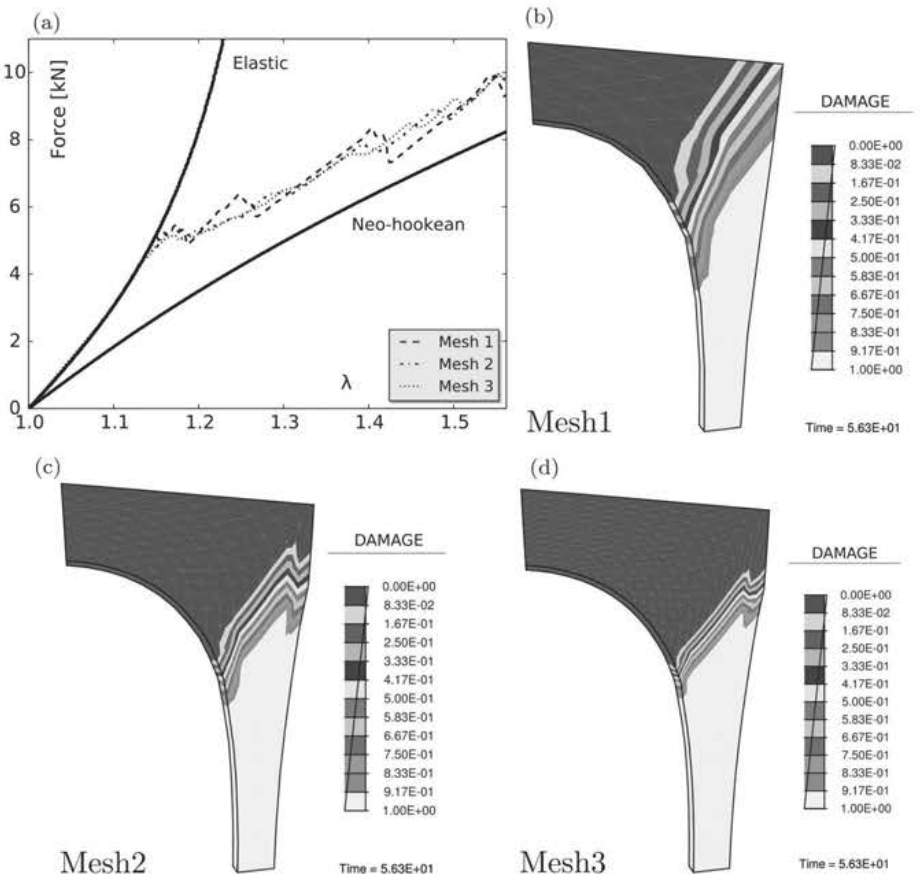

Fig. 15. (a) Force-stretch response of the model. (b) Damage contour map for discretisation *Mesh1*. (c) Damage contour map for discretisation *Mesh2*. (d) Damage contour map for discretisation *Mesh3*.

4. Discussion

The aim of this work was to establish a relationship between the mesoscopic structural mechanisms that rule inelastic processes in fibrous soft tissues and their macroscopic material parameters. A phenomenological continuous damage model with regularised softening was presented along with an interpretation of the damage processes that take place at fibril scale in soft tissues. This interpretation allows us to derive a relationship between the mechanical and geometrical properties of the fibril constituents (tropocollagen molecules and the cohesive forces between them) and the material parameters of the damage model. We have obtained meso-structurally based definitions for the elastic parameters defining the effective strain energy function, and for the inelastic parameters defining the ingredients of the damage model (yield strength and superficial density of total dissipated energy).

We have interpreted soft tissues as fibre reinforced composites and fibres as fibril reinforced composites. A Hodge-Petruska bidimensional model has been used to describe the fibrils as staggered arrays of tropocollagen molecules. After a mechanical characterisation of each of the fibril components, two fibril failures modes have been defined related with two planes of weakness. These planes of weakness are associated with either the decohesion of the distributed cohesive forces between the overlapped length of the TC molecules, or the decohesion of the concentrated cohesive forces at the end of the TC molecules. The prevailing mode of failure is a function of the TC molecular length, which allows us to characterise the fibril mechanical properties in terms of the mechanical properties of its constituents and the probability distribution of the TC molecular length. Finally, we obtain the macroscopic material properties of the fibres using an homogenisation process.

We have presented a phenomenological damage model for fibrous materials with regularised softening. Damage processes depend only on the isochoric deformation and ground matrix and fibres damage independently. We have defined a strain energy function with dilatational and isochoric contributions. The dilatational contribution has been decomposed into an isotropic part associated with the ground matrix and an anisotropic part associated with the families of fibres. We have used the principles of the smeared crack approach to avoid the mesh size dependence of the structural response in softening. We have defined a regularised softening modulus in terms of a surface density of dissipated energy and a characteristic size of the finite element.

This phenomenological damage model has been implemented as a subroutine inside the finite element code F.E.A.P. (Taylor, 2003). The process of obtaining the macroscopic material parameters from the mesoscopic fibril model was made using the environment SciPy (Jones et al., 2001).

The present approach to obtain the material parameters of the phenomenological damage model in terms of the fibril mesostructure has the advantage of its simplicity in use. The complexity of the model is reduced to an initial study to obtain the derived material parameters of the damage model without any further modification in the finite element code. We are able to incorporate the properties of the fibrous tissue structure without using the computationally more expensive multiscale models. It allows us to study the influence of the geometrical and mechanical properties of the fibril constituents in a non-expensive, straightforward way.

However, this work presents also some limitations. In the bottom-up approach we have followed, we have used the mechanical definitions (stiffness, yield strength and density per unit area of dissipated energy) of the fundamental components of soft tissues at fibril scale. These characterisations, along with the volume fractions of each component at fibre and tissue level, present a high degree of uncertainty, especially the definition of the densities per unit area of dissipated energy. Some of the numerical values considered in Tables 2–4 are based in molecular dynamics simulations, some are based in experimental tests or observations, and the others are just a choice of the authors because no experimental value has been found. A more precise geometric and mechanical characterisation is required of each of the fundamental constituents of the specific soft tissue we want to analyse.

Finally we would like to mention some limitations of the model related with the simplifying hypothesis we have considered. Firstly, we have assumed the same elastic stretch threshold for both the fibril and the fibre. This is the same as considering that fibril and fibre undergo the same strain at both length scale levels. We have also considered at fibril scale that all TC molecules deform uniformly. Intuitively we might think that in the Hodge–Petruska model there will be a stress concentration at the end of the TC molecules. Besides, we have neglected the possibility of a failure of the tropocollagen molecule when we have defined the fibril failure modes. Finally, and associated also with the fibril failure modes, we have used a distribution function of probability that can theoretically provide non-zero probability for negative values of the TC molecular length (when a standard deviation too large compared with the mean value is used, although this is a non-physiological situation).

Acknowledgement

Financial support from the Spanish Ministry of Science and Technology, through Grant DPI 2011-27609 is gratefully acknowledged.

References

Adham, M., Gournier, J.-P., Favre, J.-P., De La Roche, E., Ducerf, C., Baulieux, J., Barral, X., Pouyet, M., 1996. Mechanical characteristics of fresh and frozen human descending thoracic aorta. J. Surg. Res. 64 (1), 32–34.

Baer, E., Cassidy, J.J., Hiltner, A., 1991. Hierarchical structure of collagen composite systems. Pure Appl. Chem. 63, 961–973.

Bailey, A.J., Sims, T.J., 1976. Chemistry of the collagen cross-links. nature of the cross-links in the polymorphic forms of dermal collagen during development. Biochem. J. 153, 211–215.

Balzani, D., Schröder, J., Gross, D., 2006. Simulation of discontinuous damage incorporating residual stresses in circumferentially overstretched atherosclerotic arteries. Acta Biomater. 2 (6), 609–618.

Bhattacharjee, A., Bansal, M., 2005. Collagen structure: the madras triple helix and the current scenario. IUBMB Life 57 (3), 161–172.

Buehler, M.J., 2006a. Atomistic and continuum modeling of mechanical properties of collagen: elasticity, fracture, and self-assembly. J. Mater. Res. 21 (08), 1947–1961.

Buehler, M.J., 2006b. Nature designs tough collagen: explaining the nanostructure of collagen fibrils. Proc. Nat. Acad. Sci. 103 (33), 12285–12290.

Buehler, M.J., 2008. Nanomechanics of collagen fibrils under varying cross-link densities: atomistic and continuum studies. J. Mech. Behav. Biomed. Mater. 1 (1), 59–67.

Calvo, B., Pena, E., Martinez, M., Doblaré, M., 2007. An uncoupled directional damage model for fibred biological soft tissues. Formulation and computational aspects. Int. J. Numer. Methods Eng. 69 (10), 2036–2057.

Carson, M.W., Roach, M.R., 1990. The strength of the aortic media and its role in the propagation of aortic dissection. J. Biomech. 23 (6), 579–588.

Coleman, B.D., Gurtin, M.E., 1967. Thermodynamics with internal state variables.

Coleman, B., Noll, W., 1963. The thermodynamics of elastic materials with heat conduction and viscosity. Arch. Ration. Mech. Anal. 13 (1), 167–178.

Driessen, N., Peters, G., Huyghe, J., Bouten, C., Baaijens, F., 2003. Remodelling of continuously distributed collagen fibres in soft connective tissues. J. Biomech. 36 (8), 1151–1158.

Ehret, A.E., Itskov, M., 2009. Modeling of anisotropic softening phenomena: application to soft biological tissues. Int. J. Plast. 25 (5), 901–919.

Flory, P., 1961. Thermodynamic relations for high elastic materials. Trans. Faraday Soc. 57, 829–838.

Fung, Y., 1993. Biomechanics: Mechanical Properties of Living Tissues. Springer.

Gasser, C.T., 2011. An irreversible constitutive model for fibrous soft biological tissue: a 3-d microfiber approach with demonstrative application to abdominal aortic aneurysms. Acta Biomater. 7 (6), 2457–2466.

Gasser, T.C., Holzapfel, G.A., 2002. A rate-independent elastoplastic constitutive model for biological fiber-reinforced composites at finite strains: continuum basis, algorithmic formulation and finite element implementation. Comput. Mech. 29 (4–5), 340–360.

Gasser, T.C., Ogden, R.W., Holzapfel, G.A., 2006. Hyperelastic modelling of arterial layers with distributed collagen fibre orientations. J. R. Soc. Interface 3 (6), 15–35.

Gautieri, A., Vesentini, S., Redaelli, A., Buehler, M.J., 2011. Hierarchical structure and nanomechanics of collagen microfibrils from the atomistic scale up. Nano Lett. 11 (2), 757–766.

Holzapfel, G.A., 2000. Nonlinear solid mechanics: a continuum approach for engineering.

Holzapfel, G.A., Ogden, R.W., 2010. Constitutive modelling of arteries. Proc. R. Soc. A: Math. Phys. Eng. Sci. 466 (2118), 1551–1597.

Holzapfel, G., Gasser, T., Ogden, R., 2000. A new constitutive framework for arterial wall mechanics and a comparative study of material models. J. Elast. 61, 1–48. http://dx.doi.org/10.1023/A:1010835316564 <http://dx.doi.org/10.1023/A:1010835316564>.

Itskov, M., Aksel, N., 2004. A constitutive model for orthotropic elasto-plasticity at large strains. Arch. Appl. Mech. 74 (1–2), 75–91.

Jones, E., Oliphant, T., Peterson, P., 2001. Scipy: open source scientific tools for python. <http://www.scipy.org/>.

Kachanov, L., 1958. Time of the rupture process under creep conditions. Isv. Akad. Nauk. SSR. Otd Tekh. Nauk 8, 26–31.

Liao, J., Yang, L., Grashow, J., Sacks, M.S., 2005. Molecular orientation of collagen in intact planar connective tissues under biaxial stretch. Acta Biomater. 1 (1), 45–54.

Lorenzo, A.C., Caffarena, E.R., 2005. Elastic properties, Young's modulus determination and structural stability of the tropocollagen molecule: a computational study by steered molecular dynamics. J. Biomech. 38 (7), 1527–1533.

Martufi, G., Gasser, T.C., 2011. A constitutive model for vascular tissue that integrates fibril, fiber and continuum levels with application to the isotropic and passive properties of the infrarenal aorta. J. Biomech. 44 (14), 2544–2550.

Martufi, G., Gasser, T.C., 2012. Turnover of fibrillar collagen in soft biological tissue with application to the expansion of abdominal aortic aneurysms. J. R. Soc. Interface 9 (77), 3366–3377.

Meyers, M.A., Chen, P.-Y., Lin, A.Y.-M., Seki, Y., 2008. Biological materials: structure and mechanical properties. Prog Mater Sci 53 (1), 1–206.

Oh, B., Bazant, Z., 1983. Crack band theory for fracture of concrete. Mater. Struct. 155–177.

Oliver, J., 1989. A consistent characteristic length for smeared cracking models. Int. J. Numer. Methods Eng. 28 (2), 461–474.

Ottani, V., Raspanti, M., Ruggeri, A., 2001. Collagen structure and functional implications. Micron 32 (3), 251–260.

Peña, E., Doblaré, M., et al., 2009. An anisotropic pseudo-elastic approach for modelling Mullins effect in fibrous biological materials. Mech. Res. Commun. 36 (7), 784–790.

Peña, E., Alastrue, V., Laborda, A., Martínez, M., Doblaré, M., 2010. A constitutive formulation of vascular tissue mechanics including viscoelasticity and softening behaviour. J. Biomech. 43 (5), 984–989.

Petruska, J., Hodge, A., 1964. A subunit model for the tropocollagen macromolecule. Proc. Nat. Acad. Sci. USA 51 (5), 871.

Pierce, D.M., Maier, F., Weisbecker, H., Viertler, C., Verbrugghe, P., Famaey, N., Fourneau, I., Herijgers, P., Holzapfel, G.A., 2015. Human thoracic and abdominal aortic aneurysmal tissues: damage experiments, statistical analysis and constitutive modeling. J. Mech. Behav. Biomed. Mater. 41, 92–107.

Rodríguez, J.F., Cacho, F., Bea, J.A., Doblaré, M., 2006. A stochastic-structurally based three dimensional finite-strain damage model for fibrous soft tissue. J. Mech. Phys. Solids 54 (4), 864–886.

Sasaki, N., Odajima, S., 1996. Elongation mechanism of collagen fibrils and force–strain relations of tendon at each level of structural hierarchy. J. Biomech. 29 (9), 1131–1136.

Shen, Z.L., Dodge, M.R., Kahn, H., Ballarini, R., Eppell, S.J., 2008. Stress-strain experiments on individual collagen fibrils. Biophys. J. 95 (8), 3956–3963.

Shen, Z.L., Dodge, M.R., Kahn, H., Ballarini, R., Eppell, S.J., 2010. In vitro fracture testing of submicron diameter collagen fibril specimens. Biophys. J. 99 (6), 1986–1995.

Shen, Z.L., Kahn, H., Ballarini, R., Eppell, S.J., 2011. Viscoelastic properties of isolated collagen fibrils. Biophys. J. 100 (12), 3008–3015.

Shoulders, M.D., Raines, R.T., 2009. Collagen structure and stability. Annu. Rev. Biochem. 78, 929.

Simo, J., 1987. On a fully three-dimensional finite-strain viscoelastic damage model: formulation and computational aspects. Comput. Methods Appl. Mech. Eng. 60 (2), 153–173.

Simo, J., Ju, J., 1987. Strain-and stress-based continuum damage models – I. Formulation. Int. J. Solids Struct. 23 (7), 821–840.

Simo, J.C., Oliver, J., Armero, F., 1993. An analysis of strong discontinuities induced by strain-softening in rate-independent inelastic solids. Comput. Mech. 12 (5), 277–296.

Sommer, G., Holzapfel, G.A., 2012. 3d constitutive modeling of the biaxial mechanical response of intact and layer-dissected human carotid arteries. J. Mech. Behav. Biomed. Mater. 5 (1), 116–128.
Sommer, G., Gasser, T., Regitnig, P., Auer, M., Holzapfel, G., 2008. Dissection properties of the human aortic media: an experimental study. J. Biomech. Eng. 130, 021007.
Spencer, A., 1971. Theory of invariants. Continuum physics 1 (Part III).
Tanaka, E., Yamada, H., 1990. An inelastic constitutive model of blood vessels. Acta Mech. 82 (1–2), 21–30.
Tang, Y., Ballarini, R., Buehler, M., Eppell, S., 2010. Deformation micromechanisms of collagen fibrils under uniaxial tension. J. R. Soc. Interface 7 (46), 839–850.
Taylor, R.L., 2003. Feap – a finite element analysis program. Version 7.5 Theory Manual.
Tiessen, I., Roach, M., 1993. Factors in the initiation and propagation of aortic dissections in human autopsy aortas. J. Biomech. Eng. 115 (1), 123–125.
Ushiki, T., 2002. Collagen fibers, reticular fibers and elastic fibers. A comprehensive understanding from a morphological viewpoint. Arch. Histol. Cytol. 65 (2), 109–126.
Vorp, D., Raghavan, M., Muluk, S., Makaroun, M., Steed, D., Shapiro, R., Webster, M., 1996. Wall strength and stiffness of aneurysmal and nonaneurysmal abdominal aorta. Ann. New York Acad. Sci. 800 (1), 274–276.
Weisbecker, H., Pierce, D.M., Regitnig, P., Holzapfel, G.A., 2012. Layer-specific damage experiments and modeling of human thoracic and abdominal aortas with non-atherosclerotic intimal thickening. J. Mech. Behav. Biomed. Mater. 12, 93–106.
Wells, G., Sluys, L., 2000. Application of embedded discontinuities for softening solids. Eng. Fract. Mech. 65 (2), 263–281.